SANDIA REPORT

SAND2013-7985
Unlimited Release
September 2013

Experimental Validation of a High Voltage Pulse Measurement Method

Project Number: 170983

Stefan Cular (PI), Nishant Patel, and Darren Branch

Prepared by
Sandia National Laboratories
Albuquerque, New Mexico 87185 and Livermore, California 94550

Sandia National Laboratories is a multi-program laboratory managed and operated by Sandia Corporation, a wholly owned subsidiary of Lockheed Martin Corporation, for the U.S. Department of Energy's National Nuclear Security Administration under contract DE-AC04-94AL85000.

Issued by Sandia National Laboratories, operated for the United States Department of Energy by Sandia Corporation.

Available to DOE and DOE contractors from
U.S. Department of Energy
Office of Scientific and Technical Information
P.O. Box 62
Oak Ridge, TN 37831

Telephone: (865) 576-8401
Facsimile: (865) 576-5728
E-Mail: reports@adonis.osti.gov
Online ordering: http://www.osti.gov/bridge

Available to the public from
U.S. Department of Commerce
National Technical Information Service
5285 Port Royal Rd.
Springfield, VA 22161

Telephone: (800) 553-6847
Facsimile: (703) 605-6900
E-Mail: orders@ntis.fedworld.gov
Online order: http://www.ntis.gov/help/ordermethods.asp?loc=7-4-0#online

SAND2013-7985
Unlimited Release
September 2013

Experimental Validation of a High Voltage Pulse Measurement Method

Stefan Cular (PI) and Nishant Patel
Primary Electrical Standards Department

Darren Branch
Biosensors and Nanomaterials Department

Sandia National Laboratories
P.O. Box 5800
Albuquerque, New Mexico 87185-MS0665

Abstract

This report describes X-cut lithium niobate's ($LiNbO_3$) utilization for voltage sensing by monitoring the acoustic wave propagation changes through $LiNbO_3$ resulting from applied voltage. Direct current (DC), alternating current (AC) and pulsed voltage signals were applied to the crystal. Voltage induced shift in acoustic wave propagation time scaled quadratically for DC and AC voltages and linearly for pulsed voltages. The measured values ranged from 10 - 273 ps and 189 ps – 2 ns for DC and non-DC voltages, respectively. Data suggests $LiNbO_3$ has a frequency sensitive response to voltage. If voltage source error is eliminated through physical modeling from the uncertainty budget, the sensor's U_{95} estimated combined uncertainty could decrease to ~0.025% for DC, AC, and pulsed voltage measurements.

CONTENTS

LIST OF FIGURES

LIST OF TABLES

NOMENCLATURE

AC	alternating current
BAW	bulk acoustic wave
°C	degree Celsius
cm	centimeters
c_v	volumetric heat capacity coefficient
DC	direct current
ΔL	change in length
ΔL_{calc}	change in calculated length from COMSOL simulation
Δt	change in time
ΔT	change in temperature
dB	decibels
d_{ij}	piezoelectric coupling constant at location ij in matrix
DOE	Department of Energy
FEM	finite element modeling
f_r	frequency at resonance
HV	high voltage
J	joules
k	coverage factor
K	piezoelectric coupling constant
kHz	kilohertz
kV	kilovolt
$LiNbO_3$	lithium niobate
L_o	length of piezoelectric crystal
L_o'	length of piezoelectric crystal with added voltage induced displacement
m	meter
m_c	crystal mass
MHz	megahertz
mm	millimeter
Q	energy
µm	micrometer
µs	microsecond
NIST	National Institute of Standards and Technology
nm	nanometer
ns	nanosecond
NNSA	National Nuclear Security Administration
Ω	ohm
pm	picometer
ppb	part per billion
ppm	part per million
ps	picosecond
SAW	surface acoustic wave
SI	international standard units
t	time
U_{95}	uncertainty within 95% confidence interval

V	voltage
v_a	acoustic propagation velocity

1. INTRODUCTION

Measuring high voltage (HV) (> 10 kV) impulse systems accurately is important in determining power in electrical energy systems used in nuclear and other defense technologies, accurate beam steering in accelerators and scanning electron microscopy systems, and power metering for electrical energy distribution. To date, the technology involved in measuring pulse HV systems includes, but it not limited to: electro-optical methods using Kerr effects[1] , resistive and capacitive dividers[2, 3], surface acoustic wave (SAW) sensors[4], electro-optic modulators[5], and optical fiber voltage sensors[6]. The NIST-N1 voltage divider reference developed at the National Standards of Science and Technology (NIST), which has an uncertainty of 0.53% (k=2), is the only existing measurement artifact available for high voltage pulsed measurements[1]. The overall goal of this work is to develop a method through modeling and simulation, as well as experimental verification, to eliminate the reliance of the NIST-N1 artifact on the traceability to the SI and reduce the combined uncertainty of such measurements.

Currently, calibrated devices include capacitive and resistive dividers, which load pulse forming networks differently. The ideal device should not alter the pulse forming network. Piezoelectric crystals offer advantages important to HV sensing, which include relative high electric field breakdown voltage[7] and the ability to operate over a large frequency range. This report focuses on using the piezoelectric crystal lithium niobate, $LiNiBO_3$, as the HV sensing element. One advantage of using $LiNiBO_3$ is that it inherently has larger piezoelectric stress constants in comparison to other piezoelectric materials such as quartz and gallium arsenide[8]. This material property leads to increasing strain in the material as a result of an applied voltage. One major disadvantage to using $LiNbO_3$ is that there exists no temperature stable cut for this crystal, so the

electrical, optical, and mechanical material properties vary with temperature, on the order of 94 ppm[9]. The data presented in this report take advantage of this piezoelectric property by allowing the crystal to be utilized as a time-of-flight sensing element to measure the acoustic wave delay as a function of applied voltage. Furthermore, temperature effects were minimized by implementing sealed fixtures and operating in a tightly controlled temperature (23 ± 1 °C) environment.

Previous reports have taken advantage of the Pockels effect, and the intensity of the incoming wave versus the outgoing wave was compared to extract the applied voltage[10]. Three advantages of using acoustic waves over lasers are: 1) longitudinal acoustic waves are not polarization dependent; 2) acoustic waves are not susceptible to low frequency vibrations; 3) the cost of developing and maintaining an acoustic wave based system is generally lower. In this report, a bulk acoustic wave (BAW) element is utilized as the HV sensing element.

2. EXPERIMENTAL SETUP

2.1 Voltage Sensing Element and Fixture Configuration

The piezoelectric crystal chosen for this study was X-cut $LiNiBO_3$, with dimensions of 15 mm × 5 mm × 5 mm from Leysop Corporation. The crystal had gold electrodes on the top and bottom YZ planes. The crystal was also wrapped with a ~50 μm thick strip of copper since the voltage is applied across the long 15 mm length of the crystal. This voltage excitation was used to only distort the crystal in a longitudinal fashion. Lithium niobate crystals can handle voltages of up to 20 kV/cm[11].

The crystal was completely enclosed in a Delrin 150 fixture with dimensions 30 mm × 24 mm × 20 mm. Delrin was chosen as the fixture material because it is easy to machine, has a high volume resistivity of 10^{15} Ω-cm, and a low moisture absorption rate. As illustrated in Figure 1, the fixture contains four threaded ports for voltage or transducer inputs for separate crystal faces. The top and bottom ports are for the transducers, and the left and right ports are for the terminal connections. Threaded sleeves made from Delrin were used for terminal connections for voltage application. One transducer was threaded into the fixture directly and the other transducer was shrouded with a spring, allowing the transducer to self-align and apply a uniform orthogonal force to the end crystal face.

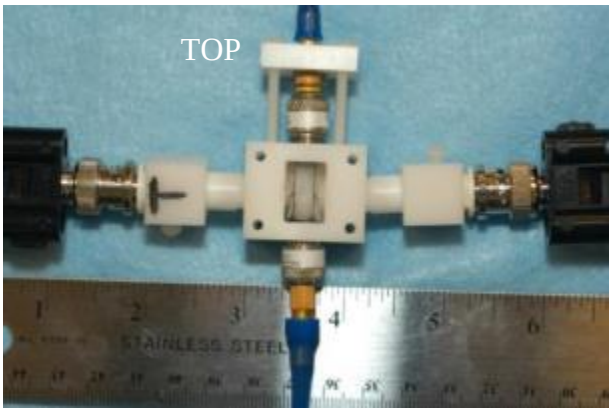

Figure 1. Crystal fixture for lithium niobate crystal with mounted transducers.

2.2 Acoustic Transducer, Crystal Characterization, and Temperature Effects on Acoustic Propagation Time

In this experiment, an acoustic wave propagates through the crystal and is monitored before, during, and after the HV was applied. The transducers operated at 10 MHz with 5 MHz in bandwidth at -6 dB and had a piezoelectric element size radius of 3 mm. The transmitting and receiving transducers used in this experiment were of the same make and model (Olympus C563). The transducers were controlled by a pulser/receiver system (Olympus 5073PR) through 1 m cables. The pulser/receiver was synchronized to a frequency/time interval counter (Stanford Research Systems SRS 620) through use of a common 10 MHz signal.

The crystal cut was verified using time-of-flight measurements to determine the acoustic velocity. The pulser/receiver unit was used to transmit and receive the acoustic wave and a Tektronix TDS3032B 300 MHz oscilloscope was used to collect the receiving transducer signal. This signal corresponded to the longitudinal wave acoustic propagation velocity, v_a= 6700 ± 200 m/s. To verify that this measured velocity was associated with a longitudinal mode, Christoffel's equation, which describes the necessary conditions for acoustic wave

propagation in a material, was solved for the modes in a 0° X-cut crystal[12]. Figure 2 (A) describes the electrical to acoustic energy conversion, *K*, within the crystal as a function of propagation angle in the crystal. Figure (B) shows the slowness curve for the different modes associated with this crystal. The longitudinal wave is denoted by the red curve and the mode solution yields a theoretical velocity of 7000 m/s (green and blue curves are shear wave modes). Figure 3 shows an oscilloscope trace of a representative output from the pulser/receiver unit used to measure the velocity. The input spike is at t = 0 s, and the acoustic wave is observed at 2.6 μs after propagating through the 15 mm crystal.

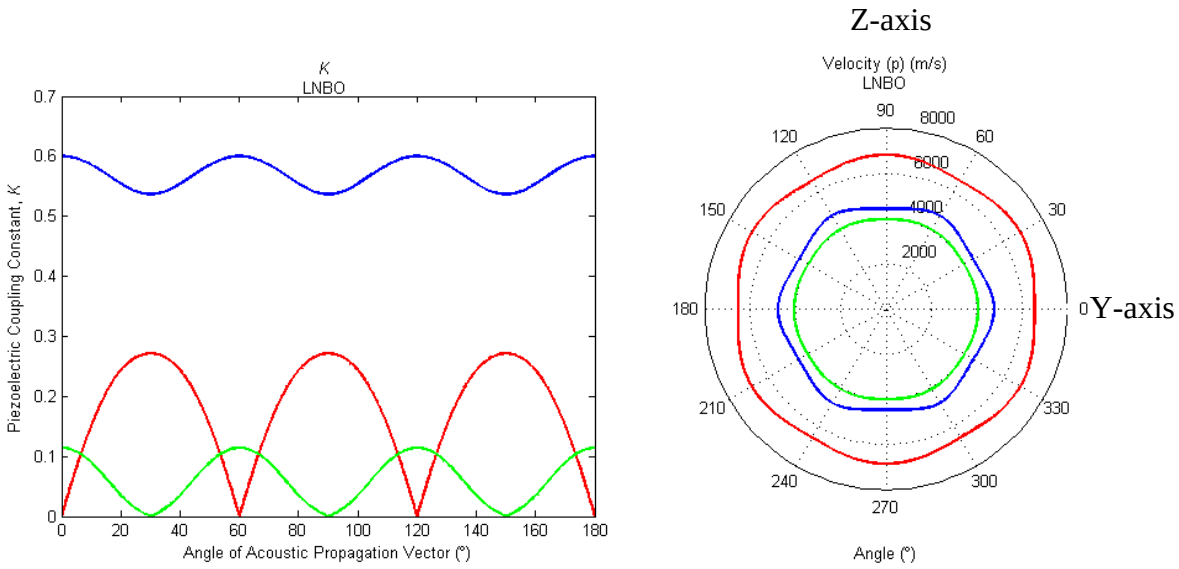

Figure 2. Solutions from solving Christoffel's equation. A) Piezoelectric constant, *K* vs. acoustic propagation vector angle for 0° X-cut lithium niobate. B) The corresponding slowness curve. The longitudinal mode is denoted by the red curve. The green and blue curves represent shear wave modes.

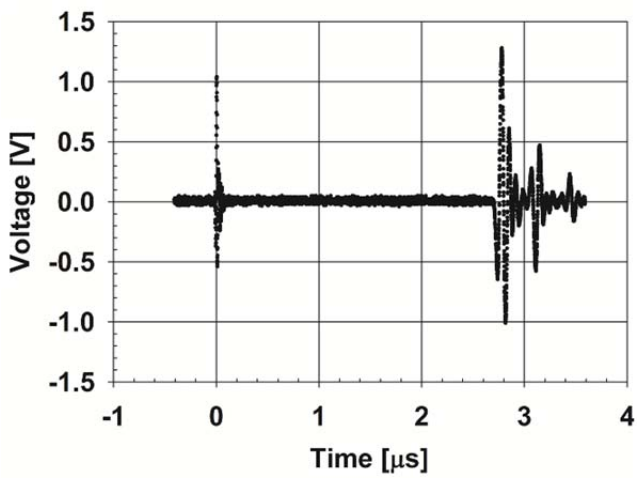

Figure 3. Time dependent voltage transducer response.

To monitor how temperature fluctuations affect the measurement, experiments were performed to monitor how the acoustic wave propagation time through the crystal with changing temperature. The temperature was varied from 20-30 °C in steps of 5 °C in a temperature controlled air bath with a Type-T thermocouple placed inside the fixture. A reference probe inside the air bath but just outside the fixture was present to determine when the system's temperature has reached equilibrium. Furthermore, the temperature was allowed to equilibrate inside with the air temperature for at least 4 hours prior to taking readings.

To determine the source heating effect's influence on the crystal response, an 1100 V DC signal was applied for 1 hour to the crystal. The amount of energy deposited onto the crystal for this time was calculated to be ~540 J based on bulk crystal properties. The specific heat equation, $Q = m_c c_v \Delta T$, was used to determine the amount of temperature change for the amount of energy dissipated, where Q is the energy, m_c is the lithium niobate mass, is the volumetric specific heat of lithium niobate, and ΔT is the temperature change. ΔT was calculated to be 0.001 °C.

2.3 Experimental Procedure

A schematic of the experimental set up is shown in Figure 4. A 1 V, 1 kHz pulse from a signal generator (HP 33250A) was used to trigger the pulser/receiver unit. The crystal was mounted in the fixture and the transducers were aligned until the receiving pulse signal amplitude was maximized. To ensure that the acoustic transducer's steel casing was not being short circuited to the crystal's gold electrodes, two 0.5 mm pieces of glass were added to both ends of the crystal for electrical isolation. Glycerin couplant was used for reducing the acoustic impedance mismatch between the transducer material and $LiNbO_3$ crystal. A time interval counter was used to measure the propagation time of the acoustic wave through the $LiNbO_3$. Fluke MET/CAL runtime was used for data collection. For AC and DC measurements, 10 minutes of no applied voltage was recorded before and after 5 minute applied voltage durations. A Fluke 5700EP multicalibrator system was used as the AC and DC voltage source, with external sense, for DC voltages UP to 1100 V and AC voltages up to 640 V at the highest possible frequency of 100 kHz.

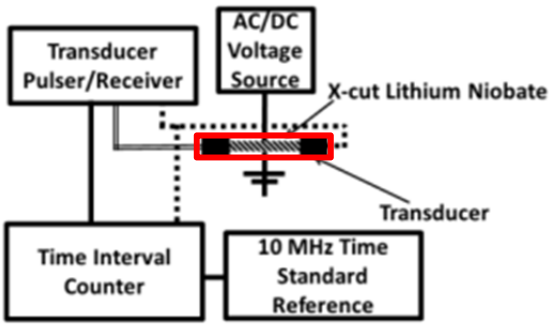

Figure 4. Schematic of experimental setup. The red box indicates the crystal fixture.

For pulse measurements, a Berkeley Nucleonics 6040 pulse generator using a Model 302H module was used for producing pulsed voltages up to 800 V with 5 µs pulse width and 100 ns

delay time. Due to the sensing element's high impedance, a 50 Ω 100 W rated resistor was placed in parallel so that the total load impedance closely matched the Model 302H 50 Ω output impedance. Ten single event pulses were performed at each voltage.

2.4 Simulation Configuration

Two different COMSOL Multiphysics models were implemented. The first model used 0° X-cut $LiNbO_3$ to calculate the static deformation of the crystal due to DC voltage. Results from the first model were fed into a second transient model, which consisted of two 10 MHz acoustic transducers and the 0° X-cut $LiNbO_3$ piezoelectric crystal. 36° X-cut $LiNbO_3$ material was used as the transducer material to mitigate any impedance mismatch between the transducer and piezoelectric crystal interface. Both 36° X-cut $LiNbO_3$ and 0° X-cut $LiNbO_3$ used the Z-X-Z definition to rotate the material properties found in the literature[13]. The Euler angles (ϕ,θ,Ψ) describe both materials by (ϕ=90°,θ=90°,Ψ), where Ψ=36° for the 36° X-cut material and Ψ=0° for the 0° X-cut material. Appendix A contains the rotated material values for both crystal orientations.

As previously mentioned, a separate model was constructed to determine the voltage induced displacement on the crystal itself. An X-cut crystal of length L_o = 0.5 mm was used. A stationary solver was used to determine the crystal deformation under DC voltage induced strain beyond breakdown based on value in ref. 10. Displacement model results were added to the crystal length in the acoustic wave propagation model, $L_{o,}$ so that a new crystal length, L_o', $L_o' = L_o + \Delta L_{calc}$ could be used for acoustic wave propagation model. The acoustic wave propagation model geometry is shown in Figure 5. The overall thickness of both the source and receiving

transducer were 0.370 mm (cross hatched portion in Figure 5), which corresponds to a transducer operating at 10 MHz. Low reflectivity boundary conditions (single hatched portions in Figure 5) were set on the lateral boundaries of the source and receiving transducer to dampen any reflections. A 10 V Heavyside step function pulse of 1 ns duration was used to stimulate a 10 MHz acoustic wave through the crystal (solid fill in Figure 5). For all transient simulations a time step of no greater than 10 ps was used.

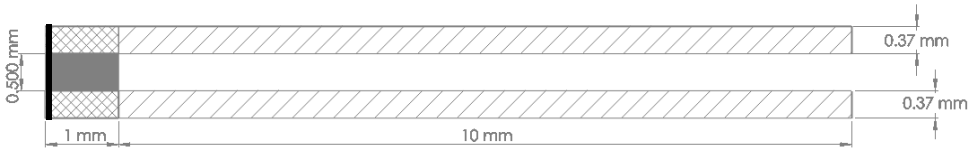

Figure 5. Model image of 2-D axisymmetric model used for COMSOL multiphysics simulation. The axis of symmetry is defined by the bold black line. The solid fill is the 0° X-cut $LiNbO_3$ material and the hashed portions are 36° X-cut $LiNbO_3$ material.

3. RESULTS AND DISCUSSION

3.1 Experimental Results

Using the time interval counter, the change in acoustic delay time between the transmitting and receiving transducer before, during, and after a voltage was applied to the crystal was monitored. Figure 6 (A) shows representative data at 640 V DC and Figure 6 (B) shows results the DC voltage results for applied voltages between 256 V-1100 V at steps of 128 V. A quadratic relationship between the applied voltage and the acoustic time delay was fitted to the data in Figure 6 (B). The error bars represent the combined standard deviation for 5 measurements at the stated applied voltage. The standard deviation ranged from 6-91 ps.

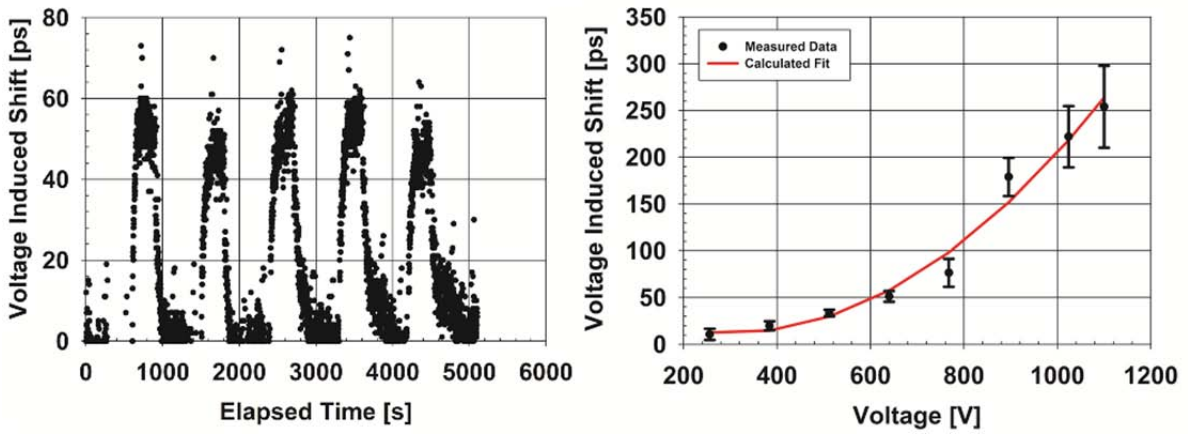

Figure 6. (A) Representative data describing voltage induced time shift vs. time of the time interval counter. (B) Lithium niobate response when DC voltage is applied.

Figure 7 shows the AC voltage results for applied voltage of 640 V for frequencies of 100 Hz-100 kHz. A quadratic relationship between the applied voltage and the acoustic time delay was observed. At frequencies under 10 kHz, the voltage induced shift doesn't change significantly within the measurement. The error bars represent the combined standard deviation for 5

measurements at the stated applied voltage. The standard deviation dropped from 91 to 20ps with increasing frequency.

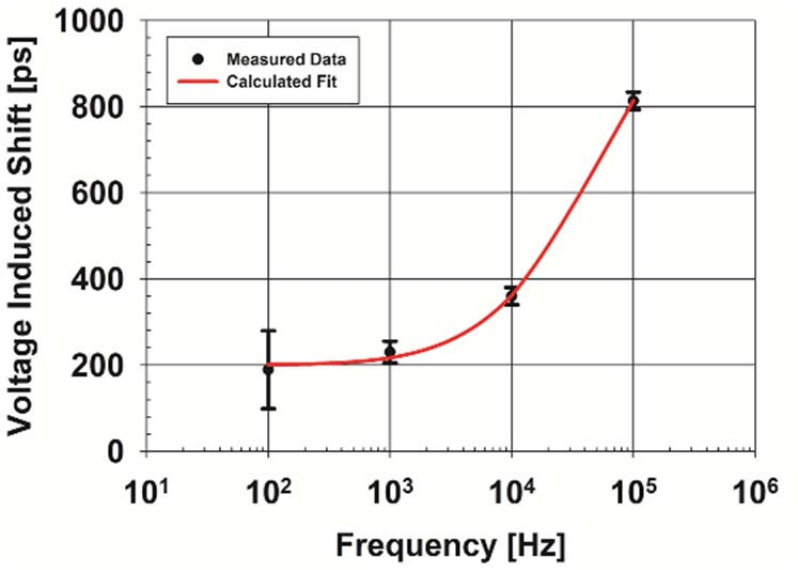

Figure 7. Lithium niobate response when AC voltage is applied.

Figure 8 (a) shows the crystal response from voltage pulses at 100, 255, 385, 640, and 800 V all with a pulse width of 5 μs. The crystal response varied from 250 ps - 2 ns. The standard deviation for the single pulsed events ranged from 29 ps to 68 ps . The single event accuracy of the time interval counter was 25 ps. The pulse width dependence on the crystal response was measured at 100 V. Figure 8(b) shows that when applying a 100 V pulse at pulse widths of 1 μs and 5 μs, there is no statistically significant change in the response data to within the measurement error of ± 50 ps. The results are tabulated and contained in Appendix B.

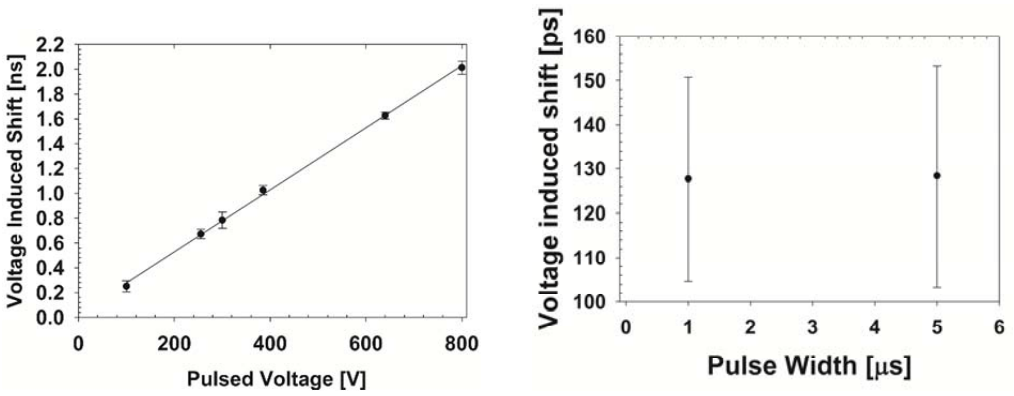

Figure 8. A) Lithium niobate response for pulsed voltages. B) Variation for induced shift as a function of pulse width for 100 V.

The acoustic propagation time with temperature variation is plotted in Figure 9. When increasing the temperature from 20 °C to 30 °C, a temperature rise by 1 °C corresponded to the acoustic wave propagation time increasing by 142 ps ± 53 ps. When the temperature was decreased from 30 °C to 25 °C, data shows 1 °C temperature decrease in temperature increased the propagation time of the acoustic wave by 94.7 ps ± 61 ps.

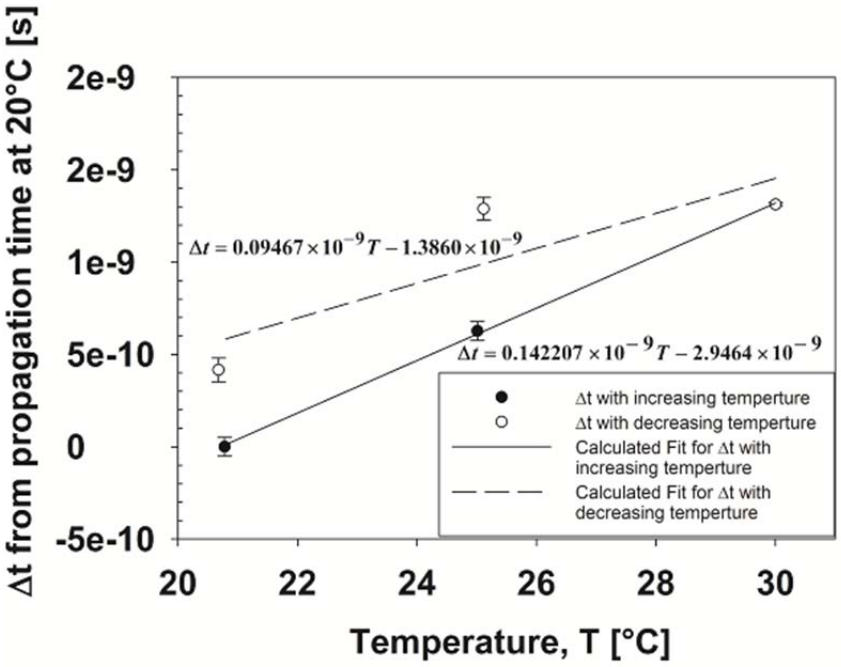

Figure 9. Acoustic wave propagation time with varying temperature.

3.2 Discussion

The acoustic wave crystal response to applied voltage ranged from 10 - 273 ps, 189 - 873 ps, and 250 ps - 2 ns for the DC, AC, and pulsed voltage measurements, respectively. Figure 10 compares the DC, AC, and pulsed voltages graphically. In comparing the AC voltage response to the DC voltage response, one can speculate that the acoustic delay time shift was influenced by frequency. Since applying DC voltage to a piezoelectric crystal results in a static deformation, the crystal does not have continuously changing stress as it would in the AC or pulsed voltage cases. Furthermore, this hypothesis is consistent with the pulsed voltage case, where the crystal interacts with all frequencies down to 200 kHz, which includes the crystal's frequency resonance, f_r, of 246.6 kHz. In the pulse measurement case, a factor of 32 increase over DC voltage at 640 V was observed in the crystal response.

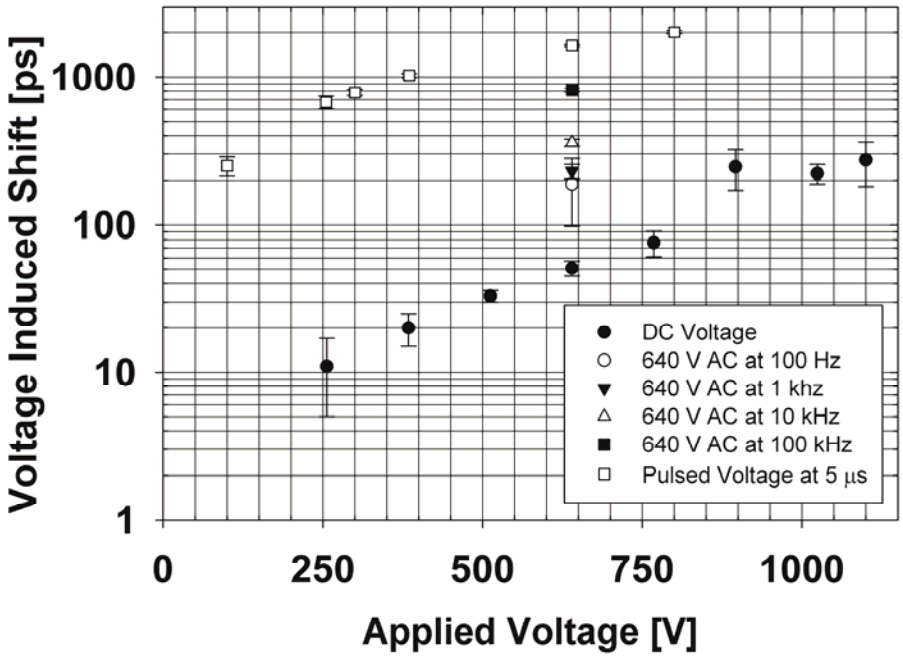

Figure 10. Voltage induced shift vs. applied voltage summary plot for DC, AC, and pulsed data in this work.

In this work, both the crystal's temperature variation due to source heating and stability of the acoustic propagation time with varying temperature were analyzed independently. With these two data sets, it was possible to ascertain how much acoustic propagation delay was associated with source heating. Combining the source heating calculation temperature change of 0.001 °C with the crystal's acoustic propagation time variation with temperature from Figure 9, it was determined that the source heating contributes at most a 0.14 ps propagation time delay to the measurement. This source heating related propagation delay is significantly smaller than the time interval counter accuracy of 50 ps, which concludes crystal heating due to energy deposition was an insignificant source of error for this work. Combining the heating and cooling coefficients from Figure 9 leads to a temperature coefficient 118 ppm/°C, which is consistent with previous literature[9].

Tables 1-3 show the uncertainty budgets for the DC, AC, and pulsed voltage measurements where the source has been removed. The largest uncertainty contribution is from the temperature fluctuations due to the crystal. If the source is included in the calculations, the expanded estimated U_{95} for DC, AC, and pulsed voltage measurements would be 0.031%, 0.121%, and 1.1%, respectively. Consequently, the percent contribution from each voltage source itself would be 1%, 76.84%, and 98.7% for DC, AC, and pulsed voltage measurements, respectively. Appendix C shows the estimated uncertainty with the voltage source included. The measurement technique used in this work was source independent, since only a time delay was being measured.

Table 1. Estimated Uncertainty Table for Crystal Response measurements for DC Voltage at V = 1100 V.

Uncertainty Description	Uncertainty Type	Standard Uncertainty	% Contribution to Combined Uncertainty
Crystal Response from DC Voltage	A	17.3 ppm	12.07%
Temperature	B	118 ppm	82.33%
Time Interval Counter	B	8.02 ppm	5.60%
10 MHz Timebase	B	0.000333 ppb	0.00%
	Estimated Expanded Combined Uncertainty, % (k=1)	0.012%	
	Estimated Expanded Combined Uncertainty, U_{95}, % (k=2.04)	0.0245%	

Table 2. Estimated Uncertainty Table for Crystal Response measurements for AC Voltage at V = 750 V and f = 100 kHz.

Uncertainty Description	Uncertainty Type	Standard Uncertainty	% Contribution to Combined Uncertainty
Crystal Response from AC Voltage	A	17.3 ppm	12.07%
Temperature	B	118 ppm	82.33%
Time Interval Counter	B	8.02 ppm	5.60%
10 MHz Timebase	B	0.000333 ppb	0.00%
	Expanded Combined Uncertainty, % (k=1)	0.012%	
	Expanded Combined Uncertainty, U_{95}, % (k=2.03)	0.0244%	

Table 3. Estimated Uncertainty Table for Crystal Response measurements for Pulsed Voltage V = 800 V at 5 μs.

Uncertainty Description	Uncertainty Type	Standard Uncertainty	% Contribution to Combined Uncertainty
Crystal Response from Pulsed Voltage	A	18.8 ppm	12.98%
Temperature	B	118 ppm	81.48%
Time Interval Counter	B	8.02 ppm	5.54%
10 MHz Timebase	B	0.000333 ppb	0.00%
	Expanded Combined Uncertainty, % (k=1)	0.012%	
	Expanded Combined Uncertainty, U_{95}, % (k=2.03)	0.0244%	

4. IMPACT

The resulting experimental data of this project show a quadratic relationship that is only seen in a few other systems. This result both complicates the physical modeling and limits the useful range of the voltage sensor, whereas a linear relationship would mitigate these issues. Varying crystalline cuts to optimize voltage response of acoustic waves is one possible route to answer this challenge. It is possible that through the use of a different cut, the crystal distortion from voltage application will possess a linear relation as well as a higher sensitivity to the applied voltage. Further techniques utilizing optical measurements are being considered as a second transduction method. Additional work is pending to complete simulation results to allow direct comparison with the reported data. These results will be used to develop simulation to experiment correlations which will then be used to investigate alternative crystalline cuts such as 36° X-Cut $LiNbO_3$, and scale the system for the desired HV range.

No programs have been directly impacted by the preliminary results of this project. With improved science and technology previously mentioned, multiple weapons programs will adopt and utilize this type of measurement technique. In particular, a number of product testers that are in the queue for supportability improvements and modernization can use this type of measurement to supplement their current capabilities.

Two direct sources of funding are being sought from the nuclear weapon community that will directly benefit from this work. A third non-NW funding source will also be sought. The first source is directly through the Primary Standards Laboratory to improve measurement capabilities to ensure the ability to support Sandia National Laboratories and other DOE/NNSA

applications. Once the foundational measurement science details have been resolved, a weapons program has agreed to tentatively fund this research through implementation into one of their product testers. The third source of funding that will be approached is the power industry via contacts at the NIST that have expressed interest in assisting to improve high voltage measurements.

5. CONCLUSION

This work reported that DC, AC, and pulsed voltage measurements were made using a piezoelectric crystal voltage sensor by monitoring acoustic wave propagation time changes with applied voltage. It was found that ns level acoustic wave propagation time shifts can be measured at moderate pulsed voltages. The estimated expanded uncertainty can be improved greater than an order of magnitude compared to the NIST-N1 divider through physical modeling to remove voltage source dependence. Due to limited project time, the experiments were not compared to simulations. More work is needed to quantify the frequency effects on voltage response, the crystal's nonlinear response to voltage stimuli, and the crystal's response at even higher voltages.

6. REFERENCES

1. FitzPatrick, G.J. and E.F. Kelley, *Comparative high voltage impulse measurement.* Journal of Research of the National Institute of Standards and Technology, 1996. **101**(5): p. 639-658.
2. Liu, Y., et al., *Design and Performance of a Resistive-Divider System for Measuring Fast HV Impulse.* Instrumentation and Measurement, IEEE Transactions on, 2011. **60**(3): p. 996-1002.
3. Jin-Liang, L., et al., *Coaxial Capacitive Dividers for High-Voltage Pulse Measurements in Intense Electron Beam Accelerator With Water Pulse-Forming Line.* Instrumentation and Measurement, IEEE Transactions on, 2009. **58**(1): p. 161-166.
4. Joshi, S.G., *Surface acoustic-wave device for measuring high voltages.* Review of Scientific Instruments, 1983. **54**(8): p. 1012-1016.
5. Huang, M.-S., M.-H. Lu, and J.-T. Shy, *High sensitivity bulk electro-optic modulator field sensor for high voltage environments.* Review of Scientific Instruments, 2004. **75**(12): p. 5364-5366.
6. Bohnert, K., M. Ingold, and J. Kostovic, *Fiber-Optic Voltage Sensor for SF_6 Gas-Insulated High-Voltage Switchgear.* Appl. Opt., 1999. **38**(10): p. 1926-1933.
7. Santos, J.C., M.C. Taplamacioglu, and K. Hidaka, *Optical high voltage measurement using Pockels microsingle crystal.* Review of Scientific Instruments, 1999. **70**(8): p. 3271-3276.
8. D.S. Ballantine, R.M.W.J., S.J. Martin, A.J. Ricco, G.C. Frye, E.T. Zellers, H. Wholtjen, *Acoustic Wave Sensors: Theory, Design and Physico-Chemical Applications*. Applications of Modern Acoustics, ed. M.L. R. Stern. 1997, New York: Academic Press.
9. Viens, M. and J.D.N. Cheeke, *Highly sensitive temperature sensor using SAW resonator oscillator.* Sensors and Actuators A: Physical, 1990. **24**(3): p. 209-211.
10. Klemme, B.J., Mahoney, A.R., *Design of an Electro-Optic Device for In-situ Measurement of High Voltage Pulses.* NCSL International Measure, 2008. **3**(2): p. 48-52.
11. Arizmendi, L., *Photonic applications of lithium niobate crystals.* physica status solidi (a), 2004. **201**(2): p. 253-283.
12. Auld, B.A., *Acoustic fields and waves in solids*. 1973, New York,: Wiley.
13. Kovacs, G., et al. *Improved material constants for $LiNbO_3$ and $LiTaO_3$*. in *Ultrasonics Symposium, 1990. Proceedings., IEEE 1990*. 1990.

APPENDIX A: MATERIAL CONSTANTS USED FOR COMSOL FEM SIMULATION

36° X-cut $LiNbO_3$

Elasticity matrix

$$\begin{bmatrix} 1.8622x10^{11}[Pa] & 8.066x10^{10}[Pa] & 6.581x10^{10}[Pa] & 0[Pa] & 0[Pa] & 0.0466x10^{11}[Pa] \\ 8.066x10^{10}[Pa] & 2.1002x10^{11}[Pa] & 5.404x10^{10}[Pa] & 0[Pa] & 0[Pa] & 0.667x10^{10}[Pa] \\ 6.581x10^{10}[Pa] & 5.404x10^{10}[Pa] & 1.9939x10^{11}[Pa] & 0[Pa] & 0[Pa] & 0.739x10^{10}[Pa] \\ 0[Pa] & 0[Pa] & 0[Pa] & 5.654x10^{10}[Pa] & -0.360x10^{10}[Pa] & 0[Pa] \\ 0[Pa] & 0[Pa] & 0[Pa] & -0.360x10^{10}[Pa] & 7.545x10^{10}[Pa] & 0[Pa] \\ 0.0466x10^{11}[Pa] & 0.667x10^{10}[Pa] & 0.739x10^{10}[Pa] & 0[Pa] & 0[Pa] & 7.518x10^{10}[Pa] \end{bmatrix}$$

Piezoelectric matrix

$$\begin{bmatrix} 4.5954[C/m^2] & -1.4209[C/m^2] & -1.7815[C/m^2] & 0[C/m^2] & 0[C/m^2] & 0.4024[C/m^2] \\ -2.3402[C/m^2] & 2.5924[C/m^2] & 1.6651[C/m^2] & 0[C/m^2] & 0[C/m^2] & 0.5717[C/m^2] \\ 0[C/m^2] & 0[C/m^2] & 0[C/m^2] & 4.4077[C/m^2] & 0.2111[C/m^2] & 0[C/m^2] \end{bmatrix}$$

Relative permittivity matrix

$$\begin{bmatrix} 38.93073 & -9.1821 & 0 \\ -9.1821 & 32.96745 & 0 \\ 0 & 0 & 45.59425 \end{bmatrix}$$

0° X-cut $LiNbO_3$

Elasticity matrix

$$\begin{bmatrix} 1.9939x10^{11}[Pa] & 6.513x10^{11}[Pa] & 5.472x10^{11}[Pa] & 0[Pa] & 0[Pa] & -0.788x10^{10}[Pa] \\ 6.513x10^{11}[Pa] & 2.279x10^{11}[Pa] & 6.513x10^{11}[Pa] & 0[Pa] & 0[Pa] & 0[Pa] \\ 5.472x10^{11}[Pa] & 6.513x10^{11}[Pa] & 1.9939x10^{11}[Pa] & 0[Pa] & 0[Pa] & 0.788x10^{10}[Pa] \\ 0[Pa] & 0[Pa] & 0[Pa] & 5.965x10^{10}[Pa] & 0.788x10^{10}[Pa] & 0[Pa] \\ 0[Pa] & 0[Pa] & 0[Pa] & 0.788x10^{10}[Pa] & 7.234x10^{10}[Pa] & 0[Pa] \\ -0.788x10^{10}[Pa] & 0[Pa] & 0.788x10^{10}[Pa] & 0[Pa] & 0[Pa] & 5.965x10^{10}[Pa] \end{bmatrix}$$

Piezoelectric matrix

$$\begin{bmatrix} 2.42[C/m^2] & 0[C/m^2] & -2.42[C/m^2] & 0[C/m^2] & 0[C/m^2] & 3.69[C/m^2] \\ 0.3[C/m^2] & 1.77[C/m^2] & 0.3[C/m^2] & 0[C/m^2] & 0[C/m^2] & 0[C/m^2] \\ 0[C/m^2] & 0[C/m^2] & 0[C/m^2] & 3.69[C/m^2] & -2.42[C/m^2] & 0[C/m^2] \end{bmatrix}$$

Relative permittivity matrix

$$\begin{bmatrix} 45.5952112 & 0 & 0 \\ 0 & 26.30449514 & 0 \\ 0 & 0 & 45.5952112 \end{bmatrix}$$

APPENDIX B: TABULATED EXPERIMENTAL RESULTS

Summary of DC Voltage Results

Voltage [V]	DC Voltage Response [ps]	Standard Deviation [ps]
256	11	6
384	20	5
512	33	3
640	51	6
768	76	15
896	246	74
1024	222	33
1100	273	91

Summary of AC Voltage Results

Frequency [Hz]	AC Voltage Response [ps]	Standard Deviation [ps]
100	189	91
1000	230	25
10000	360	20
100000	813	20

Summary of Pulsed Voltage Results with 5 μs pulse width

Pulsed Voltage [V]	Pulsed Voltage Response [ps]	Standard Deviation [ps]
100	250	36
255	672	68
300	784	37
385	1025	30
640	1628	29
800	2014	53

APPENDIX C: ESTIMATED UNCERTAINTY BUDGET WITH SOURCE INCLUDED

Table 4. Estimated Uncertainty Table for Crystal Response measurements to DC Voltages for V = 1100 V with source included

Uncertainty Description	Uncertainty Type	Standard Uncertainty	% Contribution to Estimated Expanded Combined Uncertainty
Crystal Response from DC Voltage	A	17.3 ppm	9.88%
DC Voltage Source	B	1.75 ppm	1%
Temperature	B	142 ppm	84.54%
Time Interval Counter	B	8.02 ppm	4.58%
10 MHz Timebase	B	0.000333 ppb	0.00%
	Estimated Expanded Combined Uncertainty, % (k=1)	0.0149%	
	Expanded Combined Uncertainty, U_{95}, % (k=2.04)	.0305%	

Table 5. Uncertainty Table for Crystal Response measurements to AC Voltages for V = 750 V and f = 100 kHz with the source included.

Uncertainty Description	Uncertainty Type	Standard Uncertainty	% Contribution to Combined Uncertainty
Crystal Response from AC Voltage	A	17.3 ppm	2.31%
AC Voltage Source	B	575 ppm	76.84%
Temperature	B	142 ppm	19.78%
Time Interval Counter	B	8.02 ppm	1 1.07%
10 MHz Timebase	B	0.000333 ppb	0.00%
	Estimated Expanded Combined Uncertainty, % (k=1)	.0594%	
	Expanded Combined Uncertainty, U_{95}, % (k=2.03)	0.121%	

Table 6. Uncertainty Table for Crystal Response measurements to Pulsed Voltages for V = 800 V, 5 μs pulse width with source included.

Uncertainty Description	Uncertainty Type	Standard Uncertainty	% Contribution to Combined Uncertainty
Crystal Response from Pulsed Voltage	A	18.8 ppm	0.34%
10 MHz Timebase	B	0.000333 ppb	0.00%
Temperature	B	142 ppm	2.57%
Pulsed Voltage Source	B	5370 ppm	98.66%
Time Interval Counter	B	8.68 ppm	0.09%
	Estimated Expanded Combined Uncertainty, % (k=1)	0.537%	
	Expanded Combined Uncertainty, U_{95}, % (k=2.04)	1.1%	

DISTRIBUTION

1	MS0359	D. Chavez, LDRD Office	1911
1	MS0665	R. Burton	2542
1	MS0665	S. Cular	2542
1	MS0665	N. Patel	2542
1	MS0899	Technical Library	9536 (electronic copy)
1	MS1425	D. Branch	1714
1	MS1425	S. Casalnuovo	1714


Sandia National Laboratories